Applying Horizontal Diffusion on Pressure Surface to Mesoscale Models on Terrain-Following Coordinates

HANN-MING HENRY JUANG,* CHING-TENG LEE,+ YONGXIN ZHANG,# YUCHENG SONG,@ MING-CHIN WU,+ YI-LENG CHEN,# KEVIN KODAMA,& AND SHYH-CHIN CHEN**

*Environmental Modeling Center, NCEP, Washington, D.C.
+National Taiwan University, Taipei, Taiwan
#University of Hawaii at Manoa, Honolulu, Hawaii
@RSIS/Climate Prediction Center, NCEP, Washington, D.C.
&National Weather Service Pacific Region, Honolulu, Hawaii
**Experimental Climate Prediction Center, University of California, San Diego, La Jolla, California

(Manuscript received 30 June 2003, in final form 12 August 2004)

ABSTRACT

The National Centers for Environmental Prediction regional spectral model and mesoscale spectral model (NCEP RSM/MSM) use a spectral computation on perturbation. The perturbation is defined as a deviation between RSM/MSM forecast value and their outer model or analysis value on model sigma-coordinate surfaces. The horizontal diffusion used in the models applies perturbation diffusion in spectral space on model sigma-coordinate surfaces. However, because of the large difference between RSM/MSM and their outer model or analysis terrains, the perturbation on sigma surfaces could be large over steep mountain areas as horizontal resolution increases. This large perturbation could introduce systematical error due to artificial vertical mixing from horizontal diffusion on sigma surface for variables with strong vertical stratification, such as temperature and humidity. This nonnegligible error would eventually ruin the forecast and simulation results over mountain areas in high-resolution modeling.

To avoid the erroneous vertical mixing on the systematic perturbation, a coordinate transformation is applied in deriving a horizontal diffusion on pressure surface from the variables provided on terrain-following sigma coordinates. Three cases are selected to illustrate the impact of the horizontal diffusion on pressure surfaces, which reduces or eliminates numerical errors of mesoscale modeling over mountain areas. These cases address concerns from all aspects, including unstable and stable synoptic conditions, moist and dry atmospheric settings, weather and climate integrations, hydrostatic and nonhydrostatic modeling, and island and continental orography.

After implementing the horizontal diffusion on pressure surfaces for temperature and humidity, the results show better rainfall and flow pattern simulations when compared to observations. Horizontal diffusion corrects the warming, moistening, excessive rainfall, and convergent flow patterns around high mountains under unstable and moist synoptic conditions and corrects the cooling, drying, and divergent flow patterns under stable and dry synoptic settings.

1. Introduction

It is well known that computational noise can appear for any prognostic variable after time integration in the discretized numerical modeling system. This noise could be generated because of the excessive shortwave growth through the energy cascade and aliasing of the model nonlinear integration. If noise is not reduced or controlled it could grow and eventually ruin the integration by so-called numerical nonlinear instability (Phillips 1959). There are methods to control noise. One is horizontal diffusion, which is most commonly used in numerical modeling. The other is the selected numerical difference scheme, which has intrinsic features providing diffusion implicitly—such as interpolation, which is used in the semi-Lagrangian scheme (Robert 1993)—or has enstrophy conserved, such as Arakawa's (1966) conserving difference scheme.

Diffusion schemes can be classified into two major groups. One is subscale parameterization (Tag et al. 1979, and others), which provides well-mixed fields through eddy physics, and the other is numerical smoothing (Cullen 1976; Shapiro 1970; von Storch 1978; and others). Since the horizontal scale is larger than the vertical scale in most mesoscale modeling, and the understanding of eddy physics in the horizontal direction is limited, numerical smoothing by horizontal diffusion

Corresponding author address: Dr. Hann-Ming Henry Juang, NOAA/National Sciences Center, Room 204, 5200 Auth Road, Camp Springs, MD 20746.
E-mail address: Henry.Juang@noaa.gov

© 2005 American Meteorological Society

is commonly used. To eliminate noise growth due to numerical nonlinear instability, it is sufficient to reduce only the growth of smaller-scale waves. Thus, a higher-order horizontal diffusion scheme should be used because it is more selective to the small scale. Nevertheless, as incrementally higher orders are applied, increasingly complicated and costly computations are required in gridpoint models. Thus only second- or fourth-order difference is commonly used in the gridpoint models. In a spectral model, the horizontal diffusion can be applied in spectral spaces because it is a linear term. It can even be computed in an implicit time scheme for better stability. Hence, higher-order horizontal diffusion can be readily used in the spectral model with linear computation in spectral space. For example, the National Centers for Environmental Prediction's (NCEP) operational global spectral model utilizes sixth-order horizontal diffusion at higher resolution, though it used second order with consideration of energy dissipation at lower resolutions (Kanamitsu et al. 1991).

Unlike the vertical diffusion, the horizontal diffusion term is ambiguous in terrain-following coordinates. Over mountain areas in terrain-following coordinates, should the diffusion be operated on terrain-following coordinate surfaces or horizontal height surfaces? Pielke (1984) pointed out that horizontal diffusion over mountain areas should be applied on horizontal surfaces; otherwise an erroneous vertical mixing through the horizontal diffusion on the terrain-following coordinate surfaces will occur. The error produced by this erroneous vertical mixing could be dramatically large for the variables of concern that have vertical stratification, such as temperature and humidity. In sigma-coordinate models, however, the surface pressure is a prognostic variable, and it cannot be smoothed by diffusion on the terrain surface without special treatment (Juang 1988), because surface pressure is decreasing with increase of terrain height. The direct way to avoid this kind of error is to apply horizontal diffusion on horizontal height surfaces (Zängl 2002) or quasi-horizontal pressure surfaces (Moorthi 1997; Kanamitsu et al. 2002).

Representing horizontal diffusion on horizontal or quasi-horizontal surfaces in the terrain-following coordinates requires either vertical interpolation and/or extrapolation of variables from coordinate surfaces to horizontal surfaces. However, it can be done alternatively by applying the perturbations instead of the full fields, provided that the distribution of the perturbation is not systematic or the stratification is eliminated from the perturbation. Using perturbations for horizontal diffusion on terrain-following coordinate surfaces may have some advantages. For instance, no vertical interpolation is needed; it can be expressed in one simple linear term when the computation is done in spectral space, and it is easy to apply a higher-order implicit time scheme. Perturbation methods used for horizontal diffusion on terrain-following coordinates can be an economical method, as mentioned above. This is described in section 2. However, the horizontal diffusion with perturbation on terrain-following coordinates does not work well in high-resolution modeling; thus a modified full-field horizontal diffusion on pressure surfaces is introduced in section 3. In section 4, three cases illustrate the evidences of problematic perturbation diffusion on terrain-following surfaces at high resolution. We discuss experiment design and highlight the roles of vertical stratification and atmospheric stability. In section 5, the results from these three cases are shown with comparison to diffusion on sigma surfaces, demonstrating the satisfactory solution with a full-field diffusion on pressure surfaces. Discussion and conclusions are given in section 6.

2. Perturbation horizontal diffusion on sigma coordinates

The NCEP regional spectral model (RSM) and mesoscale spectral model (MSM) are used for this study. A description of the models can be found in Juang and Kanamitsu (1994) for NCEP RSM and Juang (2000) for NCEP MSM. NCEP MSM is the nonhydrostatic version of NCEP RSM, which was developed following the same hydrostatic primitive system of model dynamics, model physics, and model structure as the NCEP global spectral model (GSM). The purpose of the perturbation method, described in detail in Juang et al. (1997), is mainly for spectral computation, as an original design. It provides a spectral truncation as well as filtering to preserve large-scale features, which is beneficial for long-term integration, as demonstrated later in Juang and Hong (2001). NCEP RSM is a hydrostatic model using sigma coordinates, and NCEP MSM is a nonhydrostatic model using hydrostatic sigma coordinates, which can be referred to as mass coordinates.

The NCEP RSM/MSM apply fourth-order horizontal diffusion on sigma surfaces to the perturbation in spectral space (Juang and Kanamitsu 1994). The perturbation equation with horizontal diffusion can be paraphrased here as the following:

$$\frac{\partial A'}{\partial t} = \left(\frac{\partial A_R}{\partial t}\right)^* - \frac{\partial A_G}{\partial t} - \kappa \nabla_\sigma^4 A', \qquad (2.1)$$

where A can be any prognostic variable and κ is a constant diffusion coefficient; A_R is a regional variable, A_G is a global variable, and A' is a perturbation defined as $A_R - A_G$. The first term on the right-hand side (rhs), $(\partial A_R/\partial t)^*$, is the total forcing computed on the regional grid without horizontal diffusion. The second term on the rhs, $\partial A_G/\partial t$, is the total tendency including outer grid diffusion from the base field of the outer model interpolated to the regional grid. The third term on the rhs is the horizontal diffusion of perturbation on a sigma surface, under the assumption that the horizontal

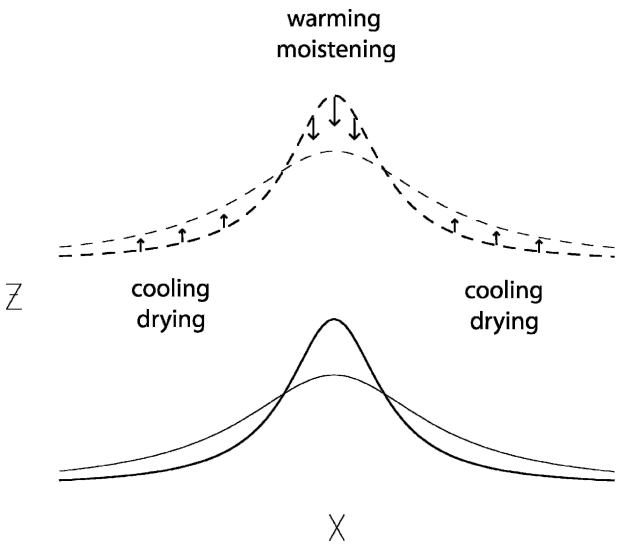

FIG. 1. A schematic plot to show the differences in height of the same sigma layers due to the model terrain differences between the outmost coarse-resolution model (light solid and dashed curves) and inner fine-resolution model (heavy solid and dashed curves). The solid curves indicate the model terrain heights, and the dashed curves indicate the model layer heights. The arrows indicate the direction of the temperature changes after applying horizontal diffusion on sigma surfaces; i.e., the temperature at heavy dashed curve will be relaxed to the value at the light dashed curve.

diffusion of the base field from the outer model has been done in the second term on the rhs (for more detail, see Juang and Kanamitsu 1994).

The perturbation horizontal diffusion on coordinate surfaces in Eq. (2.1) is a linear term and can be computed in spectral space. We can follow the procedure discussed in Sardeshmukh and Hoskins (1984) to rewrite the last term in Eq. (2.1) in spectral form for each wave as follows:

$$-\frac{1}{\tau_\sigma}\left(\frac{m^4}{M^4}+\frac{n^4}{N^4}\right)[A']_m^n, \tag{2.2}$$

where m and n are the wavenumbers, and M and N are the maximum wavenumbers in x and y directions, respectively. The $[A']_m^n$ represents the perturbation amplitude of a variable A in spectral space for wavenumber (m, n), and τ_σ is e-folding time, a weighting coefficient to control the effect of the diffusion, so that $\kappa = 1/[(\Delta x/\pi)^4\tau_\sigma]$. For numerical stability, an implicit time scheme is used:

$$\frac{([A']_m^n)^{t+\Delta t}-([A']_m^n)^{t-\Delta t}}{2\Delta t}=\left(\frac{\partial[A']_m^n}{\partial t}\right)^t-\frac{1}{\tau_\sigma}\left(\frac{m^4}{M^4}+\frac{n^4}{N^4}\right)([A']_m^n)^{t+\Delta t}, \tag{2.3}$$

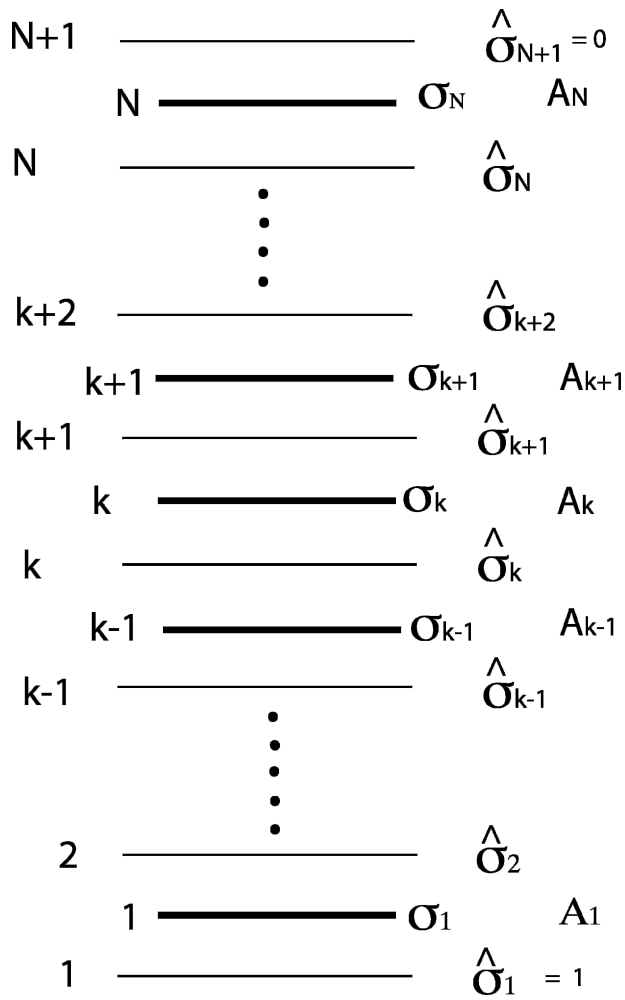

FIG. 2. The model vertical grid structure with N layers. The light solid lines indicate the model interfaces. The heavy solid lines indicate the mean value location of model layers. The interface at the bottom indicates the model ground surface. The interface at the top indicates the top of the model where pressure is zero. The variables of A used in the text are located on sigma layers; all sigmas with a "hat" are the sigma values at interfaces, and all sigmas without hats are the sigma values at layers.

where $\partial A'/\partial t = (\partial A_R/\partial t)^* - \partial A_G/\partial t$, and it can be solved as

$$([A']_m^n)^{t+\Delta t}=\frac{([A']_m^n)^{t-\Delta t}+(\partial[A']_m^n/\partial t)^t 2\Delta t}{1+\frac{2\Delta t}{\tau_\sigma}\left(\frac{m^4}{M^4}+\frac{n^4}{N^4}\right)}. \tag{2.4}$$

It can easily be seen that this form is unconditionally stable with any value of τ_σ; thus it can have a strong diffusion while τ_σ is as small as two time steps or less. It works quite well for coarse resolution when the perturbations over mountain areas are small.

The perturbation given in the previous paragraph is defined as the difference between regional model values and outer model values on the same sigma surface.

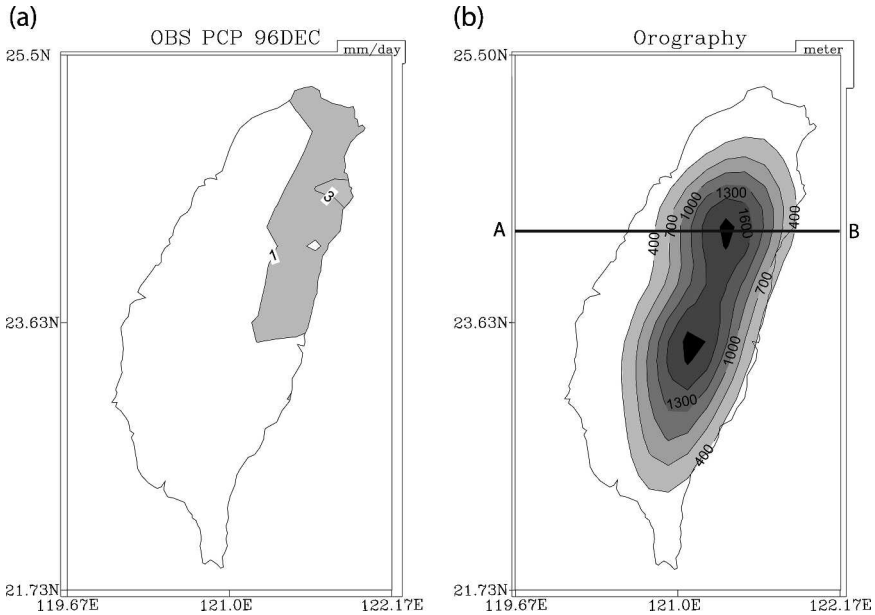

FIG. 3. (a) Monthly averaged rainfall, in mm day^{-1} with a contour interval of 2 mm day^{-1}, from observation analysis during Dec 1996. (b) The model terrain of RSM in Taiwan with horizontal resolution of 15 km.

In cases of proximity of model terrains between NCEP RSM/MSM and their outer coarse-resolution model, say NCEP GSM, the perturbation will be negligibly small initially, and the noise generated after nonlinear integration can be smoothed out by the horizontal diffusion on sigma-coordinate surfaces without introducing diffusion errors. However, as mentioned in the introduction, there is a numerical problem for horizontal diffusion on sigma surfaces over mountain areas. Although using the perturbation fields for horizontal diffusion on sigma surfaces may have less error than using the full variable, the error might still be nonnegligible near steep mountain areas when the difference in the model terrains between outer model and regional model is sufficiently large.

Figure 1 shows a schematic plot to illustrate the problem of the perturbation diffusion under normal stratification of temperature and humidity (i.e., temperature and humidity are decreasing with height). The heavy (light) solid curve and heavy (light) dashed curve indicate the heights of regional (outer) model terrain and its related sigma surface, respectively. The value on top of the high terrain in the regional model is colder and drier than that in the outer model because it represents a value at a higher altitude. Conversely, the temperature is higher and the specific humidity is larger in the regional model in a valley or at the sides of a mountain than that in the outer model because it represents a value at a lower altitude. In the inverted stratification (temperature and humidity are increasing with height), the condition is reversed. With the described pattern of perturbation in normal stratification or vice versa in inverted stratification, the horizontal diffusion of perturbation on a sigma surface will reduce the perturbation, that is, reduce the difference between the regional model and the outer model; hence perturbation diffusion causes warming (moistening) on top of a mountain and cooling (drying) over the sides of a mountain or in a valley under a normal stratification, and cooling (drying) on top of a mountain and warming (moistening) in a valley or at the sides of a mountain under an inverted stratification.

The errors by perturbation diffusion can be modified (enhanced or reduced) under two atmospheric conditions that differ because of ambient stabilities. In case of a conditional unstable atmosphere under normal stratification, it is favorable to the warming and moistening on top of mountains, where the warming/moistening air induces convection with rainfall. The diabatic heating due to convection enhances its warming and induces additional convergence around the mountain, which provides warm/humid air to mix with erroneous cold/dry air at the sides of a mountain or in a valley; hence the cold/dry air due to perturbation diffusion error will be reduced. In case of a stable atmosphere under normal stratification, the warm and moistening air on top of the mountain may try to ascend but the ambient conditions from the stable atmosphere prohibits its growth; thus there is no convergence induced as described in an unstable atmosphere. Therefore the cooling and drying air in a valley or on the sides of a mountain keep accumulating without mixing as described in an unstable atmosphere; hence, it has to flow down the hill and spread to the oceans

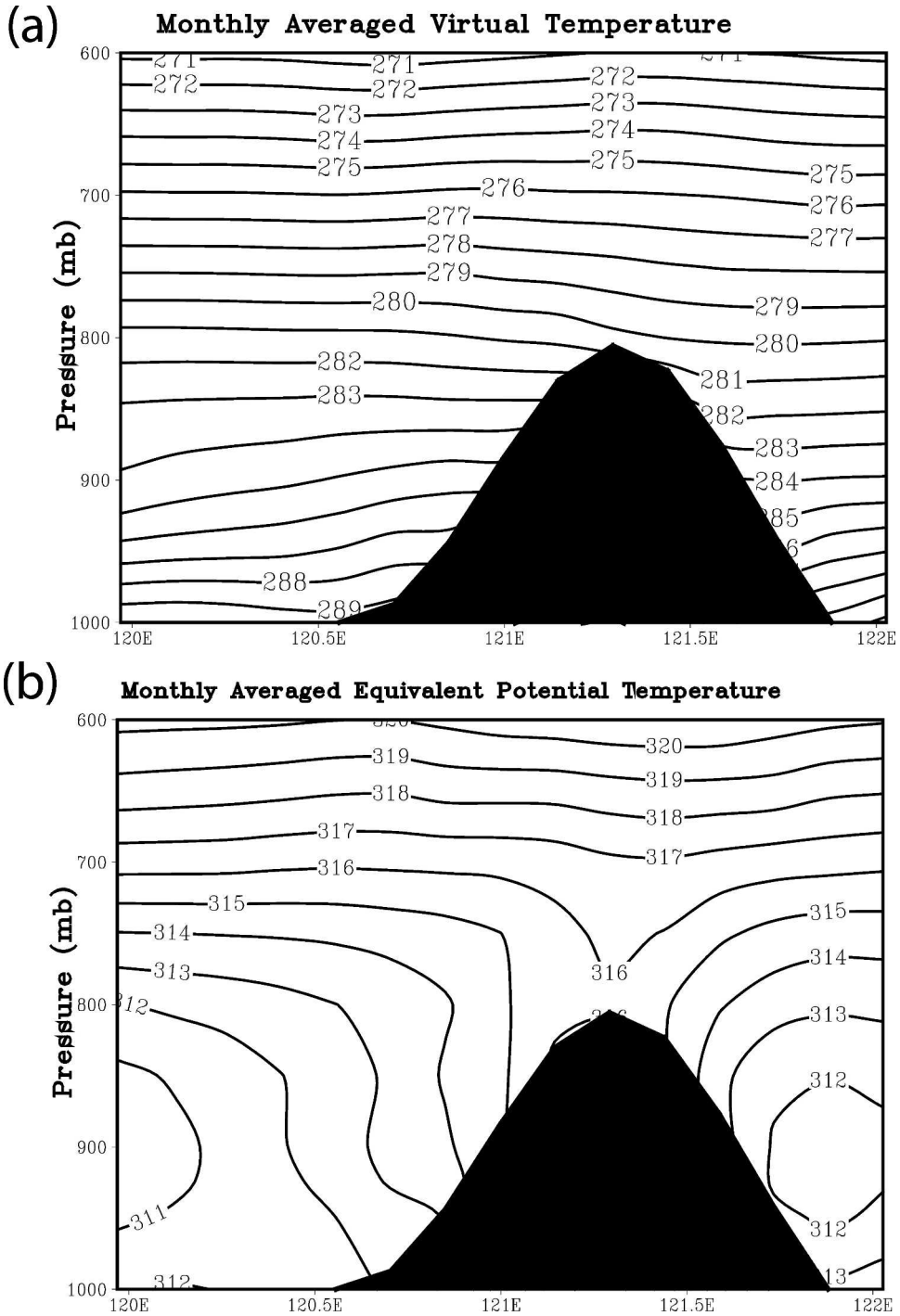

FIG. 4. Vertical cross sections of (a) monthly average virtual temperature and (b) equivalent potential temperature with contour intervals of 1 K at the location indicated in Fig. 3b.

because it is heavier than the environmental air. Thus the cold and dry portion is enhanced. These hypotheses and outcomes due to stratification and stability are examined and discussed in sections 4 and 5 with three real cases.

Furthermore, Fig. 1 can be used to depict full-field diffusion as well. The horizontal diffusion on the sigma surfaces with full fields (either heavy dashed curve for regional model or light dashed curve for outer model) will induce warming and moistening (cooling and drying) on top of mountains and cooling and drying (warming and moistening) over valleys because of the

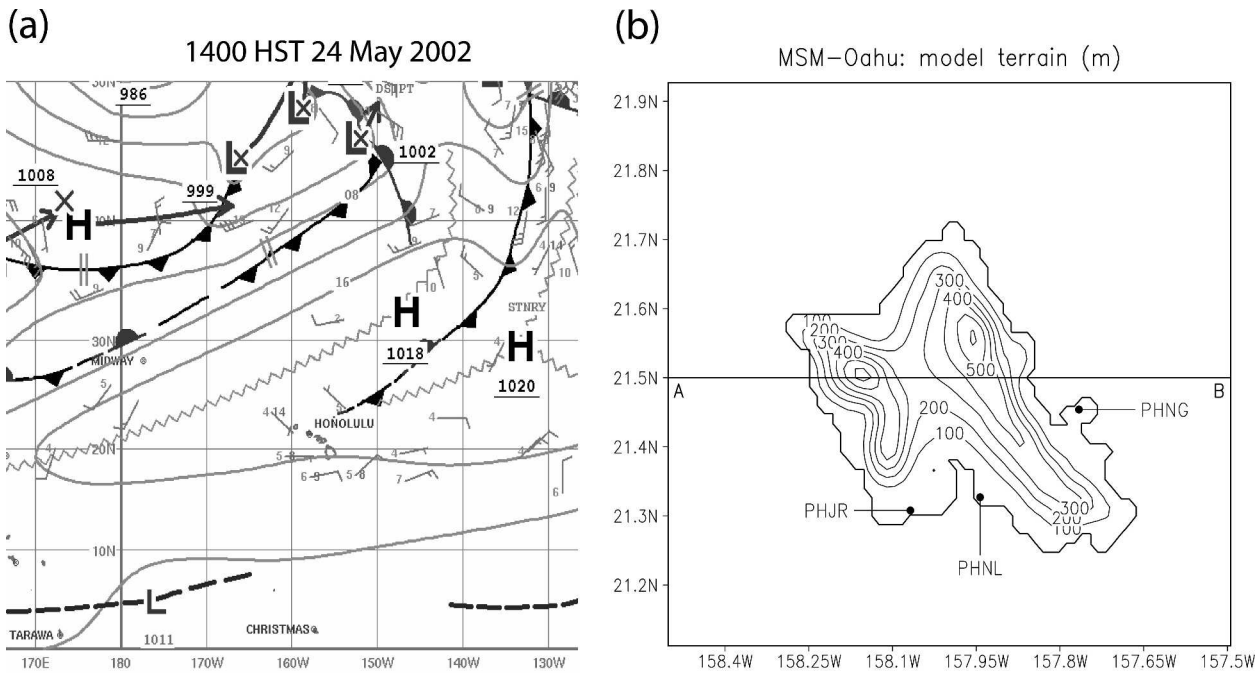

FIG. 5. (a) The synoptic weather chart over the Hawaiian Islands on 1400 HST 24 May 2002. (b) The NCEP MSM model terrain, in m with contour intervals of 100 m, over the island of Oahu, HI, for the experiment with 1.5-km horizontal resolution. PHJR, PHNL, and PHNG are three observed stations.

vertical mixing on sigma coordinates under a normal stratification (an inverted stratification).

3. Horizontal diffusion on pressure surfaces in sigma coordinates

As mentioned, when the NCEP RSM and MSM increase their horizontal resolution, the terrain difference between the regional models and their outer models, say NCEP GSM or coarser-resolution NCEP RSM/MSM, increases significantly. Thus numerical error from erroneous horizontal diffusion on sigma surfaces will appear because of the large perturbation differences over the mountain area. Eventually it ruins the forecast or simulation. The immediate solution, instead of modifying the definition of perturbation, is to apply diffusion on horizontal or quasi-horizontal surfaces, such as constant height or pressure surfaces, respectively. For the predicted variables in NCEP RSM/MSM, only temperature and moisture require modification because of their systematic stratification. The horizontal and vertical wind field, and nonhydrostatic pressure in NCEP MSM, are not always monotonically increasing or decreasing with height, so they can be diffused on sigma surfaces for smoothing purposes. Surface pressure does not require horizontal diffusion because it is computed by integrating the total column of the divergence of the smoothed wind fields.

Since sigma coordinates are related to pressure in NCEP RSM/MSM, it is easier to use a pressure surface as the quasi-horizontal surface for horizontal diffusion rather than a height surface. Because of the complexity of derivation involved in fourth-order difference, a second-order diffusion scheme is used. It is known that fourth-order diffusion is more scale selective. However, we used a relatively small diffusion coefficient for the second-order scheme. Second-order diffusion on a pressure surface can be written as

$$\kappa\nabla_p^2 A = \kappa\left(\frac{\partial^2 A}{\partial x^2} + \frac{\partial^2 A}{\partial y^2}\right)_p, \tag{3.1}$$

where A can be either temperature or specific humidity, and κ is a constant coefficient. To use it on a sigma surface, we apply a coordinate transformation:

$$\left(\frac{\partial A}{\partial x}\right)_p = \left(\frac{\partial A}{\partial x}\right)_\sigma - \left(\frac{\partial A}{\partial P}\right)\left(\frac{\partial P}{\partial x}\right)_\sigma, \tag{3.2}$$

where $P = \sigma P_s$. We use $\ln(P_s)$ in the model, so Eq. (3.2) can be rewritten as

$$\left(\frac{\partial A}{\partial x}\right)_p = \left(\frac{\partial A}{\partial x}\right)_\sigma - \left(\frac{\partial A}{\partial \ln\sigma}\right)\left(\frac{\partial \ln P_s}{\partial x}\right)_\sigma. \tag{3.3}$$

The second derivative can be written by differentiating Eq. (3.3). For simplicity, the subscript for sigma sur-

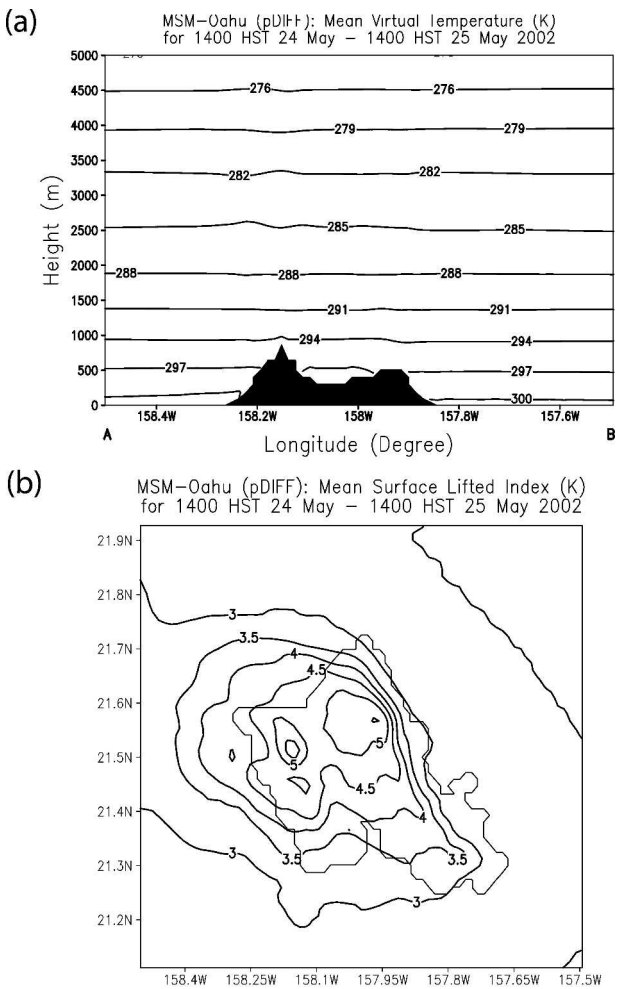

FIG. 6. (a) Vertical cross section of daily mean virtual temperature with contour intervals of 3 K at the location indicated in Fig. 5b, and (b) daily mean surface-lifted index with contour intervals of 0.5 K for 24 May 2002.

faces is dropped on the right-hand side hereafter. Then we get

$$\left.\frac{\partial\left(\frac{\partial A}{\partial x}\right)_p}{\partial x}\right|_p = \frac{\partial\left(\frac{\partial A}{\partial x} - \frac{\partial A}{\partial \ln\sigma}\frac{\partial \ln P_s}{\partial x}\right)}{\partial x} - \frac{\partial \ln p_s}{\partial x}\frac{\partial\left(\frac{\partial A}{\partial x} - \frac{\partial A}{\partial \ln\sigma}\frac{\partial \ln P_s}{\partial x}\right)}{\partial \ln\sigma}. \tag{3.4}$$

After further manipulation, we get

$$\left.\frac{\partial^2 A}{\partial x^2}\right|_p = \frac{\partial^2 A}{\partial x^2} - \frac{\partial A}{\partial \ln\sigma}\frac{\partial^2 \ln P_s}{\partial x^2} - 2\frac{\partial^2 A}{\partial \ln\sigma \partial x}\frac{\partial \ln P_s}{\partial x} + \frac{\partial^2 A}{\partial \ln\sigma^2}\left(\frac{\partial \ln P_s}{\partial x}\right)^2. \tag{3.5}$$

We can obtain the same form of Eq. (3.5) in the y direction. Then, the final equation we need for second-order diffusion can be written as

$$\nabla_P^2 A = \nabla_\sigma^2 A - \frac{\partial A}{\partial \ln\sigma}\nabla_\sigma^2 \ln P_s - 2\frac{\partial}{\partial \ln\sigma}\left(\frac{\partial A}{\partial x}\frac{\partial \ln P_s}{\partial x} + \frac{\partial A}{\partial y}\frac{\partial \ln P_s}{\partial y}\right) + \frac{\partial^2 A}{\partial \ln\sigma^2}\left[\left(\frac{\partial \ln P_s}{\partial x}\right)^2 + \left(\frac{\partial \ln P_s}{\partial y}\right)^2\right]. \tag{3.6}$$

For spectral computation on sigma surfaces, which is different from the finite-difference method, all the horizontal differentials on the rhs in Eq. (3.6) are discretized at grid point (i, j): first the spectral coefficients of A and $\ln P_s$ are used to compute their derivatives in spectral space, then they are transformed into a gridpoint space at point (i, j) by spectral transform. Then, all vertical differentials are discretized by a second-order finite difference as follows:

$$\left.\frac{\partial A}{\partial \ln\sigma}\right|_k = 0.5\left(\hat{\sigma}_{k+1}\frac{A_{k+1} - A_k}{\sigma_{k+1} - \sigma_k} + \hat{\sigma}_k\frac{A_k - A_{k-1}}{\sigma_k - \sigma_{k-1}}\right) \tag{3.7}$$

and

$$\left.\frac{\partial^2 A}{\partial \ln\sigma^2}\right|_k = \frac{\sigma_k}{\hat{\sigma}_{k+1} - \hat{\sigma}_k} \times \left(\hat{\sigma}_{k+1}\frac{A_{k+1} - A_k}{\sigma_{k+1} - \sigma_k} - \hat{\sigma}_k\frac{A_k - A_{k-1}}{\sigma_k - \sigma_{k-1}}\right), \tag{3.8}$$

where sigma hat is sigma at the interface, and sigma without hat is sigma at the layer where variable A is located; see Fig. 2 for the vertical grid structure. Note that all terms in the discretization of nonlinear computation for the spectral model are evaluated at point (i, j, k). For example, the second term in Eq. (3.6), the Laplacian of $\ln P_s$, is computed by the spectral method as described using the gridpoint value at point (i, j, k). The vertical gradient of A is computed by Eq. (3.7) and also obtained value at point (i, j, k). Then, the value of the second term in Eq. (3.6) at point (i, j, k) is the product of the Laplacian of $\ln P_s$ and the vertical gradient of A; both are evaluated (or discretized) at point (i, j, k). Furthermore, the condition of a zero vertical gradient of A at top and bottom boundaries is assumed.

Because of the nonlinear terms in Eq. (3.6), an explicit time-integration scheme is used for the diffusion, and the diffusion is evaluated at the $t-\Delta t$ step for stability in leapfrog time differencing:

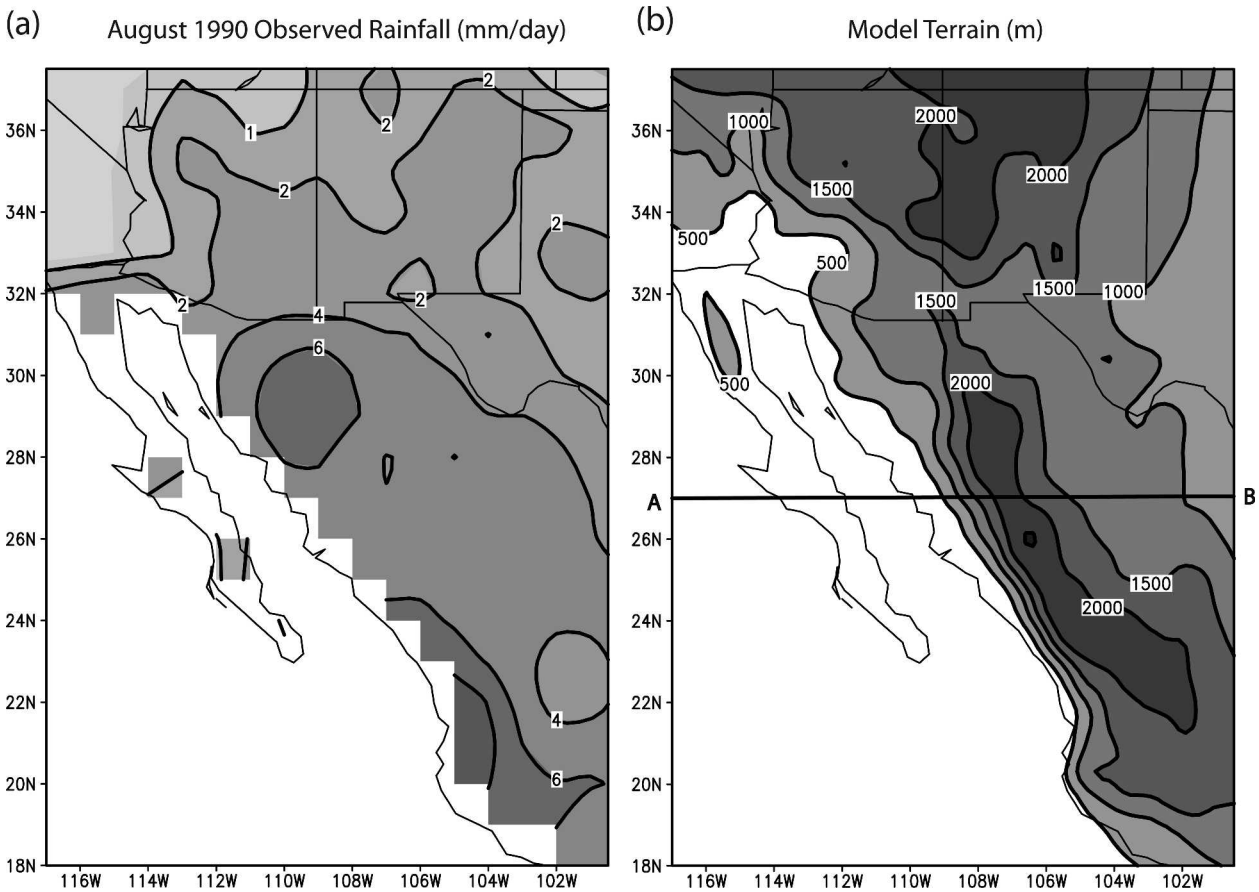

FIG. 7. (a) Monthly averaged observed rainfall rates, in mm day^{-1} with a contour interval of 1, 2, 4, and 6 mm day^{-1}, during Aug 1990. (b) NCEP RSM model terrain, in m with contour intervals of 500 m, for the experiment with 20-km horizontal resolution.

$$\frac{(A')^{t+\Delta t} - (A')^{t-\Delta t}}{2\Delta t} = \ldots\ldots + \frac{\mu}{\tau_p}\nabla_P^2 (A')^{t-\Delta t}, \qquad (3.9)$$

where $\mu = 0.125(\ \ x)^2$ (ignoring any map factor for simplicity); τ_p should be a value in seconds larger than $2\ \ t$; and $\kappa = \mu / \tau_p$ is from Eqs. (3.9) and (3.1). Furthermore, the last term in Eq. (3.6) is higher than quadratic. Although the model has enough grid points to resolve a quadratic term in the spectral transform, it may not be free of aliasing. However, the results from experiments with and without aliasing (not shown here) are similar.

Since RSM/MSM use relaxation to eliminate lateral boundary noise, the diffusion along the lateral boundary may not be necessary. Thus, a blending coefficient, α (Juang and Kanamitsu 1994), is applied to $\mu = 0.125\alpha(\ \ x)^2$ in order to reduce the diffusion along the lateral boundary.

4. Case descriptions and experimental design

Three cases are selected from three different geographic locations. They are selected from three RSM/MSM working groups. Nevertheless, each case represents the problem of diffusion on sigma surfaces in its own aspect. This section describes each case in terms of its mean virtual temperature stratification and stability during the entire period of model integration. Virtual temperature field is shown in this section because that is the field used in the model for horizontal diffusion, and its stratification determines the locations of positive and negative temperature biases over the mountain area as described in section 2 with Fig. 1. Hereafter "s-DIFF" refers to the original fourth-order scheme, and "p-DIFF" represents the full-field second-order horizontal diffusion on pressure surfaces as described in section 3.

a. Wintertime rainfall over Taiwan

During December of 1996, the eastern edge of the Siberian high provides a prevailing northeasterly wind over Taiwan and vicinity. The north–south-oriented mountain range over the center of the island, reaching elevations around 3000 m, lifted the prevailing northeasterly wind to produce rainfall over northeastern Tai-

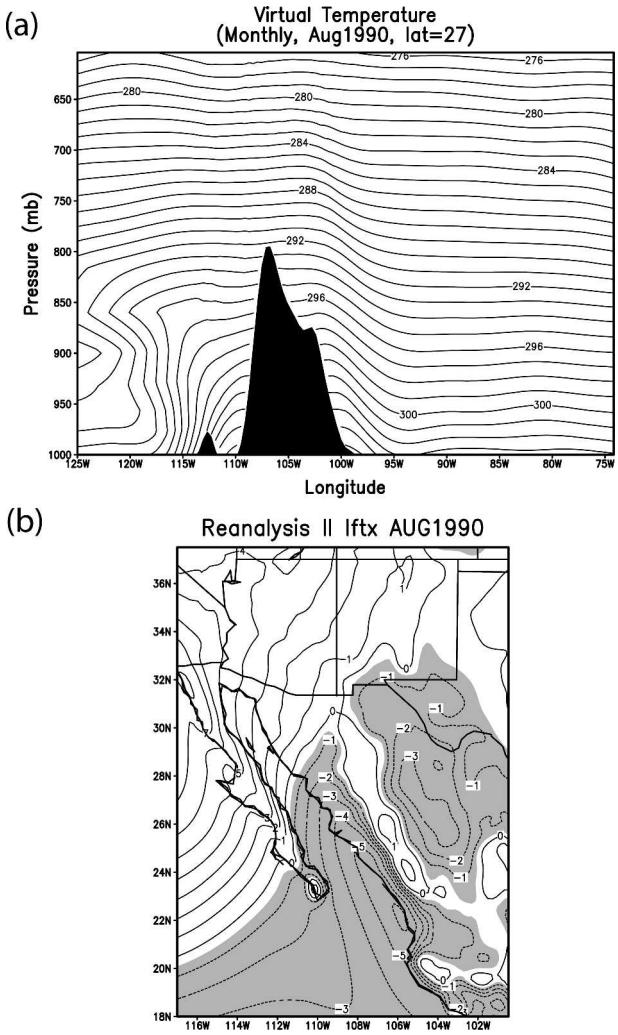

FIG. 8. (a) Vertical cross section of monthly mean virtual temperature with contour intervals of 1 K at the location indicated in Fig. 7b, and (b) surface-lifted index with contour intervals of 1 K for Aug 1990.

wan (see Fig. 3a). Figure 3b shows the smoothed model terrain with two peaks, only about 2000 m high, obtained by interpolating from Navy–National Center for Atmospheric Research (NCAR) 5′× 5′ topography data. The line indicated by A and B is the location of a vertical cross section used to examine stratification and stability later.

Both s-DIFF and p-DIFF schemes were applied to the NCEP RSM for a 1-month integration. Reanalysis data (Kalnay et al. 1996)—T62 and 28 layers—provided the initial and boundary conditions. Two simulations with two nested grids are performed; the first nested grid is from global reanalysis to 50-km p-DIFF NCEP RSM, and the second nested grid is from 50-km p-DIFF to either s-DIFF or p-DIFF 15-km NCEP RSM. The 50-km p-DIFF was used for both 15-km runs because the 50-km p-DIFF simulation was considered better than the 50-km s-DIFF. In addition, it is reasonable to compare 15-km runs between s-DIFF and p-DIFF using the same base fields of 50-km p-DIFF. The initial condition is on 1 December 1996, and lateral boundary conditions and the base fields were updated every time step by interpolation of values of outer model results or analysis at 6-h intervals. The time step for 15 km is 60 s, and the diffusion *e*-folding time, τ_p, is 1800 s.

We use model-integrated results to examine the stratification and stability of this case, because model-integrated results represented the responses during the integration. Figure 4a shows monthly averaged virtual temperature, which has normal stratification (temperature decreases with height). The temperature difference between mountaintop and foothill is about 9 K. However, the monthly mean equivalent potential temperature shows a conditionally unstable condition over oceans, and a near-neutral condition along the mountain surface layer in Fig. 4b. This case is a shallow unstable atmosphere near the ground with normal stratification. Both s-DIFF and p-DIFF simulations show the same patterns in terms of stratification and shallow unstable surface layers. We use equivalent potential temperature instead of surface-lifted index in this case because the shallow unstable surface layers cannot be detected by the surface-lifted index while the midatmosphere is stable.

b. Weak trade wind condition over the island of Oahu

A weak trade wind weather forecast case over Hawaii was selected. Figure 5a shows the synoptic chart over Hawaii on 0000 UTC 25 May 2002 [i.e., 1400 Hawaii standard time (HST) 24 May 2002]. It indicated a high pressure center (1018 hPa) about 10° northeast of Oahu with a weak pressure gradient around the Hawaiian Islands, which provided a weak trade wind condition with benign weather. Figure 5b shows the model terrain with a contour interval of 100 m over the island of Oahu. The line indicated by A and B is the location for the vertical cross section shown for this case later.

The NCEP global analysis (T170, 42 layers) on 0000 UTC 25 May 2002 was used as the initial condition. NCEP global model forecasts were used as the boundary conditions at 6-h intervals. First, NCEP RSM with 10 km was nested within the global model forecasts, and RSM outputs were at every 3 h. Then NCEP MSM with 1.5 km was nested within 10-km NCEP RSM. All models are running with 28 vertical layers. The model terrain was interpolated from Navy–NCAR 1 km by 1 km topographic data and truncated with the model resolution. The time step for the 1.5-km NCEP MSM run was 6 s, and the diffusion coefficient was 2400 s. The total integration period was 1 day.

For the same reason given in the previous case, we checked the stability and stratification. Figure 6a shows

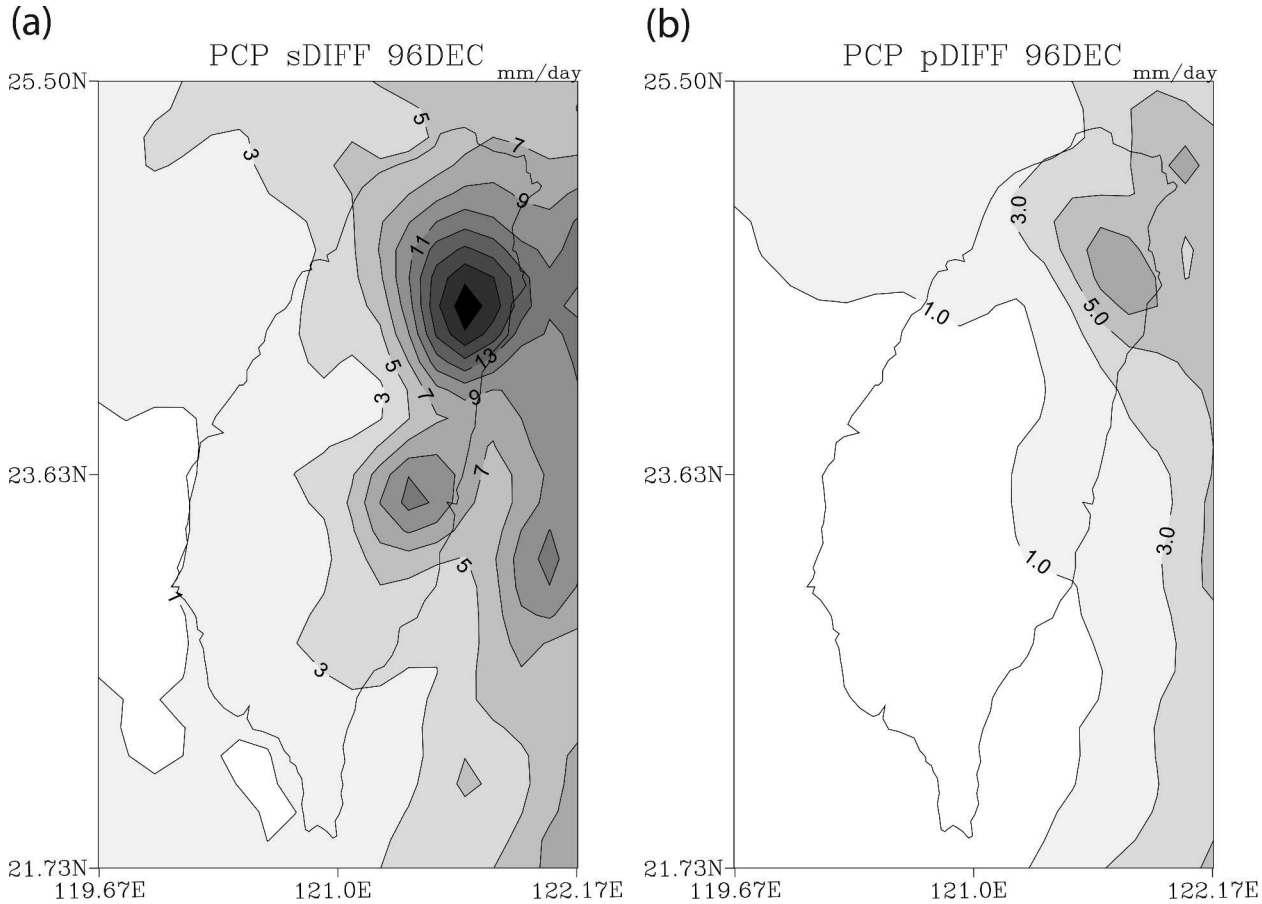

FIG. 9. Monthly averaged rainfall rates, in mm day^{-1} with a contour interval of 2 mm day^{-1}, for Dec 1996 from NCEP RSM with (a) perturbation fourth-order horizontal diffusion on sigma surfaces and (b) full-field second-order horizontal diffusion on pressure surfaces.

the daily mean virtual temperature. We can see that there is normal stratification in virtual temperature throughout the whole cross section. Figure 6b shows mean surface-lifted index from p-DIFF during 1-day integration. The definition of lifted index used here is the temperature difference (Tenv − Tpar) between environment temperature (Tenv) and lifted air parcel temperature (Tpar) on 500 hPa. The air parcel temperature on 500 hPa is obtained by lifting air at the first model layer upward adiabatically, then moist adiabatically after it is saturated, up to the 500-hPa surface. Results from s-DIFF have slightly different values from those from p-DIFF, but both values are all positive. This, shown in Fig. 5b, indicates a stable atmosphere, with no permanent temperature inversion during the 1-day integration period.

c. *Summer monsoon rainfall over North America*

This is a North America summer monsoon case over Mexico and the southwest U.S. states of Arizona and New Mexico (AZNM). Figure 7a shows the model domain and the monthly averaged observed rainfall rate in mm day^{-1} for August 1990. Figure 7b shows the model terrain with a contour interval of 500 m. The line indicated by A and B is the location of the vertical cross section used in this case. Figure 7a shows that there was a rainfall rate exceeding 4 mm day^{-1} in nearly all of Mexico, with two maxima above 6 mm day^{-1}: one around the northwestern portion of the Sierra Madre Occidental, and the other around the southwestern valleys along the coast. The rainfall rate around 2 mm day^{-1} over the southern portion of AZNM indicates the northern edge of the monsoon surge from Mexico (Anderson et al. 2000).

The NCEP–NCAR reanalysis data (Kalnay et al. 1996) were used as the initial condition, the lateral boundary, and the base field for NCEP RSM. The resolution of the NCEP RSM was 20 km in the horizontal and 28 layers in the vertical. The NCEP RSM performed a 1-month integration starting on 1 August 1990 with sea surface temperature updated daily. The time step of the model was 120 s, and the diffusion time scale was 6000 s.

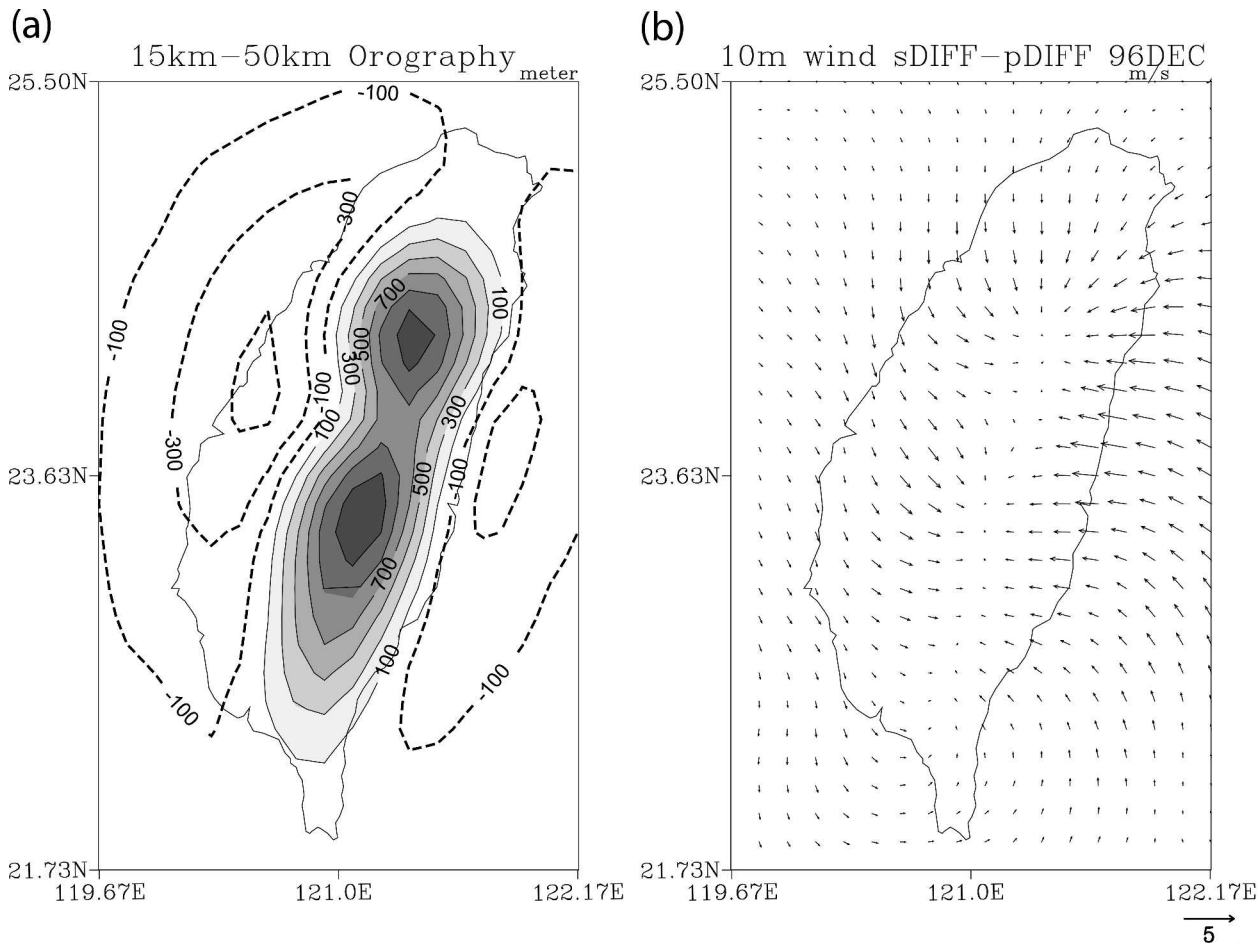

FIG. 10. (a) The terrain difference in meters between 15- and 50-km RSM, which is the base field for 15-km RSM. (b) The difference of monthly averaged 10-m wind in m s^{-1} between experiments of horizontal diffusion on sigma surfaces and on pressure surfaces for Dec 1996.

In this case, the synoptic condition was more complicated. Its stratification and stability are shown in Fig. 8. Virtual temperature decreased with altitude everywhere except west of Baja California and over the Pacific Ocean. The stratification was neutral over the west of Baja California, and an inversion up to 900 hPa was over the Pacific Ocean. The plot of surface-lifted index shows two areas of negative values, which indicate unstable atmospheric conditions, and the atmosphere is stable over Baja California, the Pacific Ocean, northern Mexico, and the remaining states in Fig. 8. Thus this case presents multiple conditions for examining the responses of s-DIFF and p-DIFF simulations.

5. Results

The results of the p-DIFF scheme for each case are compared to those from the original s-DIFF scheme. The differences in simulation will be cross-referenced to the stratification and stability discussed in the previous section.

a. Taiwan case

Figure 9 shows the monthly averaged rainfall rate with a contour interval of 2 mm day^{-1} from (a) the experiment with s-DIFF and (b) the experiment with p-DIFF. Although both experiments result in excessive rainfall as compared to observations in Fig. 3a, the locations of the local maxima of the rainfall rate are well predicted. The result from p-DIFF (in Fig. 9b) improves the simulation by reducing the excess rainfall amount of the s-DIFF experiment by half (in Fig. 9a) and changes from two local maxima in s-DIFF to one maximum in p-DIFF as in the observations.

Figure 10a shows the model terrain difference between the 15-km RSM and the 50-km RSM, which provides the base field for the 15-km RSM. All of Taiwan is covered with positive values except the western side and the coastal waters. A vertical cross section in the east–west direction over Taiwan would show the patterns as in Fig. 1. Figure 10b reveals the wind difference between the experiments with s-DIFF and p-DIFF.

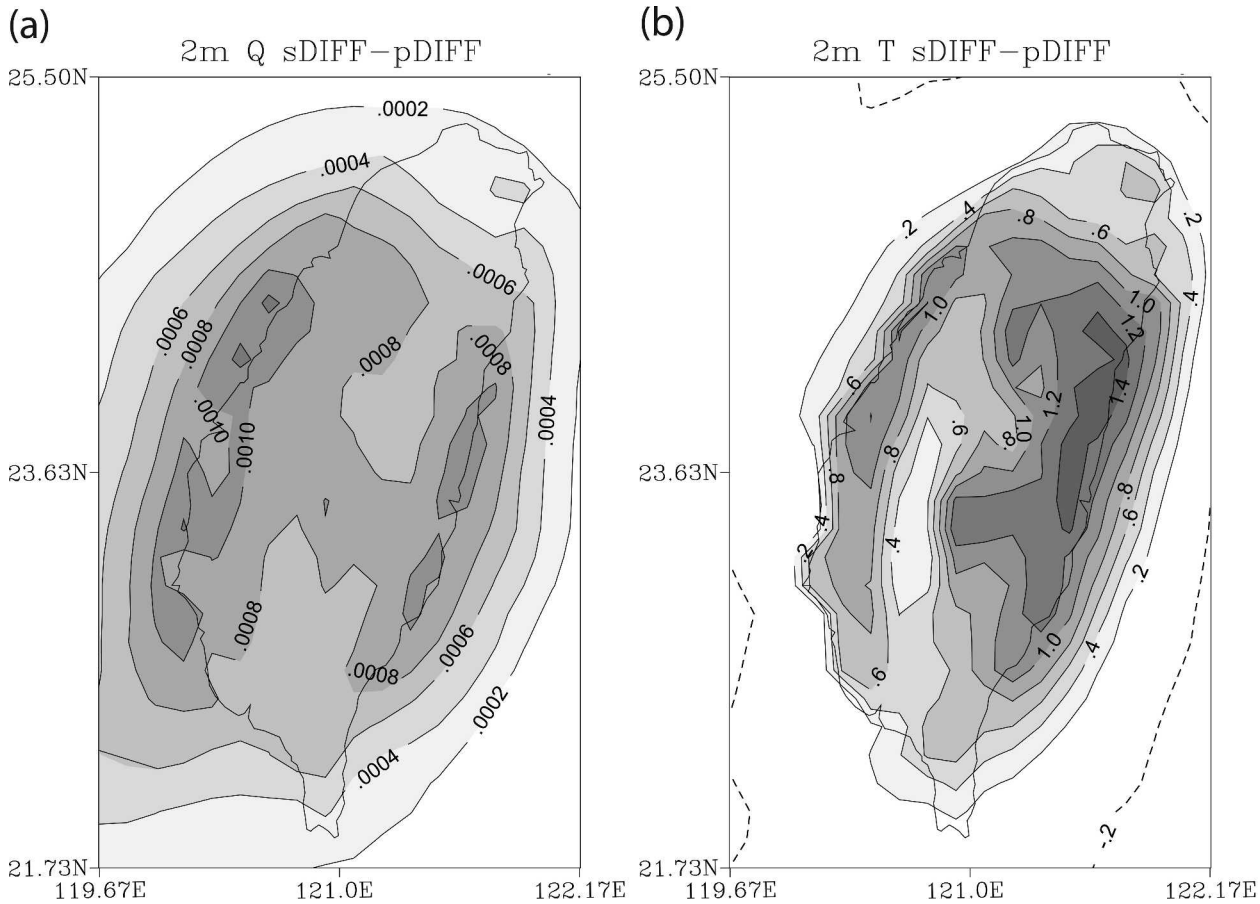

FIG. 11. The differences for monthly averaged (a) 2-m specific humidity in g g^{-1} with a contour interval of 2 10^{-4} g g^{-1} and (b) temperature with contour intervals of 0.2 K between the experiment with horizontal diffusion on sigma surfaces and the experiment with horizontal diffusion on pressure surfaces for Dec 1996.

There is a clear indication that the flow difference inclines to move toward the top of the mountains due to the impact of the horizontal diffusion on sigma surfaces, with convergence near mountaintops on the windward side.

Figure 11 shows the differences between the experiment with s-DIFF and the experiment with p-DIFF for (a) 2-m specific humidity with a contour interval of 0.0002 g g^{-1} and (b) 2-m temperature with a contour interval of 0.2 K. It indicates that the s-DIFF simulations were warmer and more humid with the maximum values around onshore and coastal areas, as shown in Fig. 11a. Thus, the s-DIFF under this condition results in erroneously high moisture and temperature over mountain areas, which leads to excessive rainfall; p-DIFF corrects these erroneous results, with reduced and more reasonable rainfall.

b. Island of Oahu case

In the clement weather condition described in section 4b, a land–sea breeze should be expected on Oahu due to the effect of the diurnal cycle. Figure 12 shows the model 10-m wind valid at 2000 HST 24 May 2002 after a 6-h integration, from experiments of (a) s-DIFF and (b) p-DIFF. It clearly indicates that this entire domain is under an averaged trade wind of 5 m s^{-1}, but the local wind patterns in the two experiments are dramatically different, not only over the island but also over the nearby coastal waters. At 2000 HST, the land–sea breeze is normally in its sea-breeze phase (see Chen et al. 2003). Thus, it is quite easy to identify the erroneous flow pattern in Fig. 12a, which shows a strong land breeze over the windward side. However, after the modification of the horizontal diffusion on pressure surfaces, the flow has a reasonable pattern without a land breeze on the windward side and a remarkable leeside wake, as shown in Fig. 12b.

The difference in 2-m temperature between s-DIFF and p-DIFF is shown in Fig. 13a, and the corrected 2-m temperature by p-DIFF is shown in Fig. 13b after a 6-h integration. Results from Fig. 13a indicate that the air in s-DIFF is warmer at the mountaintop and colder along the valleys of the mountains, and that the accu-

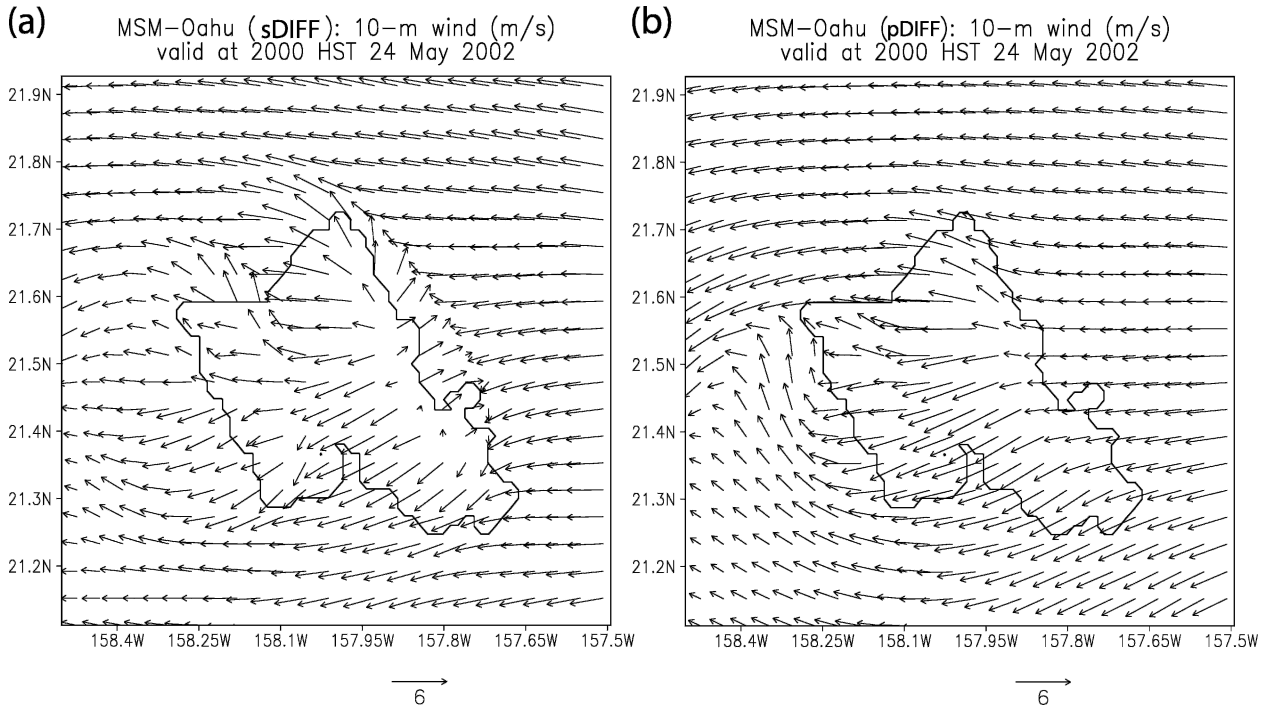

FIG. 12. The 6-h forecast 10-m wind field in m s^{-1} valid at 2000 HST 24 May 2002 from (a) the experiment with perturbation fourth-order horizontal diffusion on sigma surfaces, and (b) from the experiment with full-field second-order horizontal diffusion on pressure surfaces.

mulated cold air spreads into the coastal waters on the windward side. The location of the warming center is slightly west of the mountaintop (see Fig. 13c). This downstream shift may be because of advection by the prevailing wind. The stable atmosphere, as shown in section 4b, provides a favorable condition for a large area of erroneous cooling along the hills, which results in a downslope erroneous land breeze by s-DIFF. As discussed in section 2 and shown in Fig. 5a, the high pressure center provides favorable conditions to enhance the cooling portion and to induce downslope airflow under normal stratification by the effect of s-DIFF.

Figure 14 shows the difference for 2-m specific humidity. The distribution of specific humidity differences between s-DIFF and p-DIFF indicates more aridity along hills and coastal waters and more humidity on mountaintops as shown in Fig. 14a. The pattern of the specific humidity on the experiment with p-DIFF in Fig. 14b represents a reasonable result. Again, the locations of the local maxima of moistening are shifted by the prevailing wind, slightly more than those of temperature shown in Fig. 13a. Given the similar mountain differences as in the previous case in Fig. 10a as well as the prototype in Fig. 1, and under the normal stratification, the temperature and humidity differences in this case demonstrate similar patterns as those described in Fig. 1. But the resulting errors due to s-DIFF are quite different in appearance, especially the wind field. In the Taiwan winter case, warming and moistening of the s-DIFF simulation over high ground were enhanced by the condensation due to the excess moisture in the shallow unstable ambient atmosphere, and the resulting wind field produced a convergent difference pattern in support of the condensation over the top of the mountain. In the Oahu weak trade wind case, however, no precipitation was produced in either experiment. The warming and moistening on the mountaintop does not trigger convection due to the stable atmosphere, rather, it vertically mixed with upper cold air since it is lighter than the environment. The accumulated cooling and drying biases covered most of the slope and foothill areas, which induces heavier air than the environment so that the cool/dry air flows downhill and spreads over coastal oceans. Basically, the ambient atmospheric stratification and the error produced in temperature/humidity fields by s-DIFF are similar in both the Taiwan and Oahu cases. However, the difference in ambient stability results in uneven amplification in error patterns for both cases. Thus stability plays a key role in explaining the enhancement of the errors due to s-DIFF.

c. *North America case*

Figure 15 shows the monthly averaged rainfall rate, mm day^{-1}, for August 1990 from (a) the experiment with s-DIFF and (b) the experiment with p-DIFF. Both results show local rainfall maxima all over AZNM and Mexico, but s-DIFF results in more erroneous features

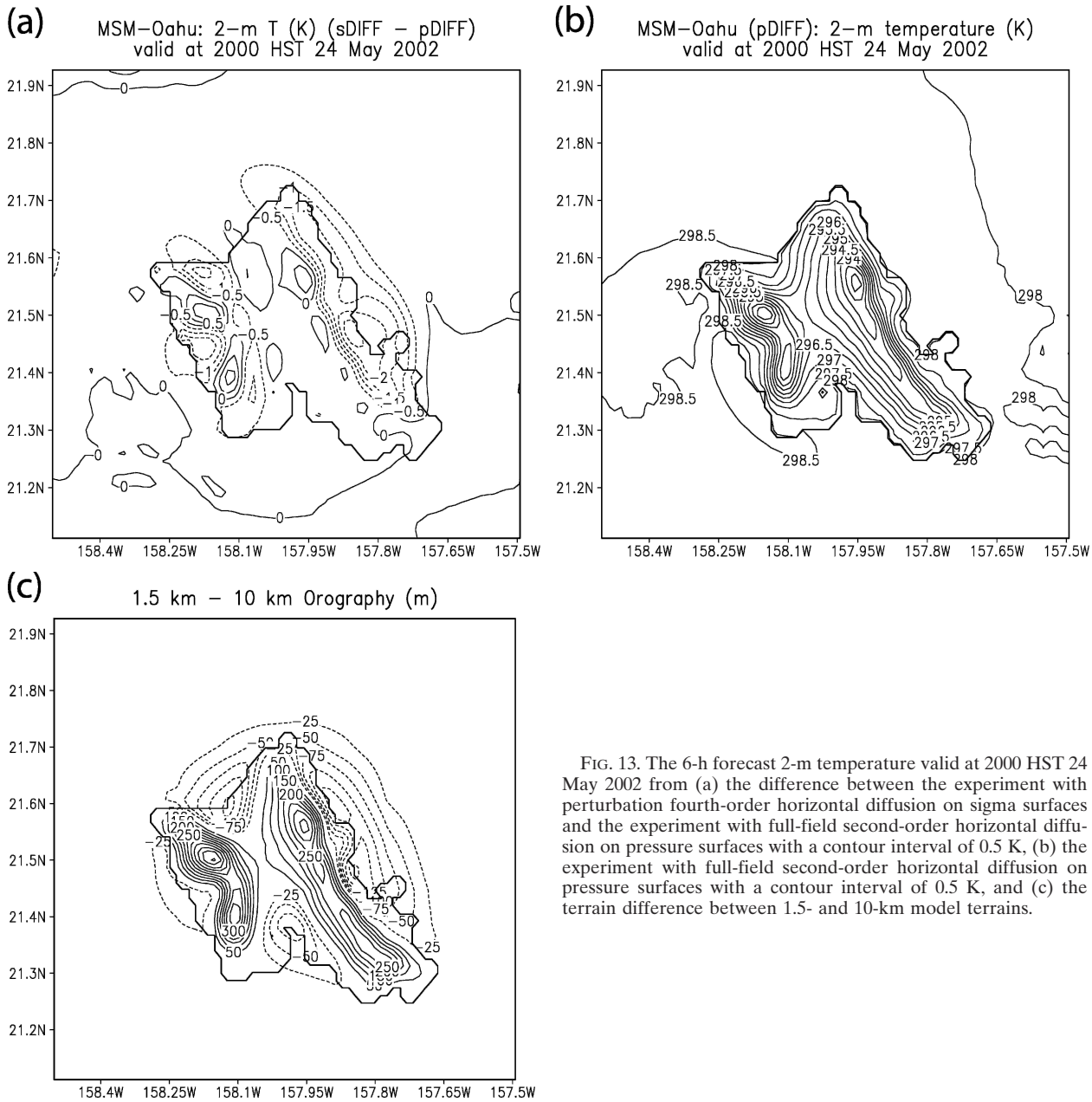

FIG. 13. The 6-h forecast 2-m temperature valid at 2000 HST 24 May 2002 from (a) the difference between the experiment with perturbation fourth-order horizontal diffusion on sigma surfaces and the experiment with full-field second-order horizontal diffusion on pressure surfaces with a contour interval of 0.5 K, (b) the experiment with full-field second-order horizontal diffusion on pressure surfaces with a contour interval of 0.5 K, and (c) the terrain difference between 1.5- and 10-km model terrains.

than p-DIFF as compared to the observations shown in Fig. 7a. The results from s-DIFF, in Fig. 15a, show a narrow area of 4 mm day^{-1} rainfall rate over Sierra Madre Occidental, and the local maximum rainfall rates are on top of high mountains. The results from p-DIFF in Fig. 15b show larger areas of rainfall above 4 mm day^{-1} over the northern Sierra Madre Occidental and southwestern portions of the mountains. Over AZNM, the results from p-DIFF in Fig. 15b show more rainfall than those from s-DIFF in Fig. 15a, and the pattern of rainfall in Fig. 15b is much closer to the pattern of observed rainfall in Fig. 7a than those in Fig. 15a.

Figure 16 shows the differences in (a) model terrains between 20-km RSM and T62 GSM and (b) precipitable water between the experiments of s-DIFF and p-DIFF. Nearly the entire domain has a negative precipitable water difference, except the areas of the Sierra Madre Occidental in Fig. 16b. This is consistent with the rainfall pattern in Fig. 15a and the terrain differences in Fig. 16a, where most rain falls over high-terrain areas from the experiment s-DIFF because of the erroneous convergence of flow by diffusion on sigma surfaces. The result from the p-DIFF experiment has no erroneous convergence to move moisture trapped at the high terrains; thus it has more precipitable water all

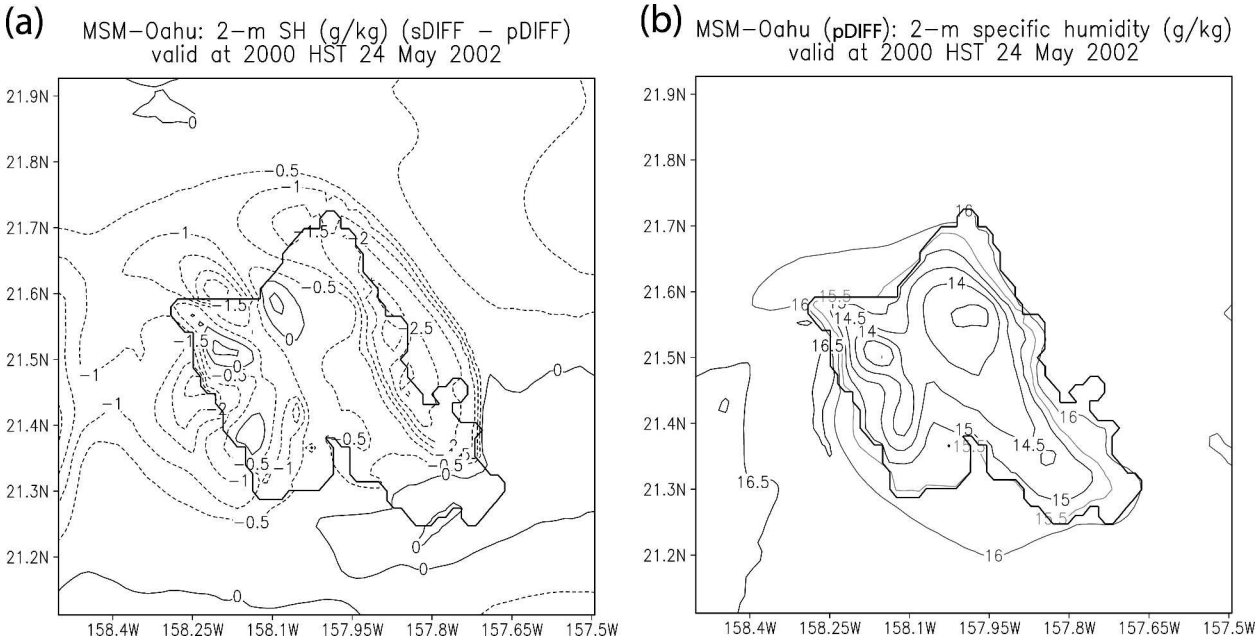

FIG. 14. (a), (b) Same as Figs. 13a and 13b, except for 2-m specific humidity with a contour interval of 0.5 g kg^{-1}.

over the region as shown in Fig. 16a and more widespread rainfall in Fig. 15b.

In this case, the atmosphere was stable over the northwestern portion of the model domain including Arizona, New Mexico, southern California, the Pacific Ocean, and Baja California, and conditionally unstable atmosphere existed over the remaining regions as evident from the rainfall patterns and Fig. 8b. These two conditions result in the same differences between the flow patterns and temperature fields as in the previous two cases, as represented by the difference fields between s-DIFF and p-DIFF and shown in Fig. 17. Over Baja California (stable conditions) with a terrain difference of about 200 m shown in Fig. 16a, the s-DIFF simulation erroneously generated cool air (2-m temperature difference in Fig. 17b) and produced downslope, land-breeze-type 10-m winds (Fig. 17a), as in the case of the Oahu simulation. Over the remaining unstable atmosphere domain, similar to the Taiwan case, upslope wind and warming from s-DIFF dominated. Furthermore, p-DIFF and s-DIFF simulations produce southward wind over the Gulf of California and the western slope of the Sierra Madre Occidental (not shown), but the difference in Fig. 17a indicates that s-DIFF simulation has less magnitude of southerlies over the areas of the major monsoon surge. Thus p-DIFF should give a better monsoon surge than s-DIFF.

It can be further demonstrated that p-DIFF is better than s-DIFF by examining the daily rainfall evolution over AZNM (from –112° to –102°W and from 32° to 36°N) shown in Fig. 18. The daily rainfall during August 1990 over AZNM as observed (solid curve), and simulations using p-DIFF (dotted curve) and s-DIFF (dashed curve) are shown. Although the model with s-DIFF and p-DIFF schemes failed to simulate the event on 21 August, it successfully picked up the other two major events, one on 6 August, the other during 14–15 August. Also, the major event with largest rainfall had a precipitation amount up to 12 mm day^{-1}, which is correctly simulated in the p-DIFF experiment. This suggests that p-DIFF produced a better simulation resulting in a correct amount of rainfall. Furthermore, most of the precipitable water was trapped over the Sierra Madre Occidental by s-DIFF, depriving the downstream area, AZNM, and hence producing less rainfall there.

6. Conclusions and discussions

A modified horizontal diffusion is implemented in NCEP RSM and MSM to replace the original method. Although the original method is a computationally efficient scheme, it can be managed in spectral space with a more stable implicit time scheme, and it is more scale selective because it is a fourth-order diffusion. It produces erroneous rainfall and flow patterns in higher-resolution modeling. Because of the definition of the perturbation in NCEP RSM/MSM, the systematic errors become nonnegligible as the horizontal resolution increases, when the deviations from the driving outer model increase over mountain areas. Consequently, the original perturbation diffusion scheme produces erroneous results when it is applied on sigma surfaces, though it is generally considered a reasonable scheme for the coarse resolution of NCEP RSM.

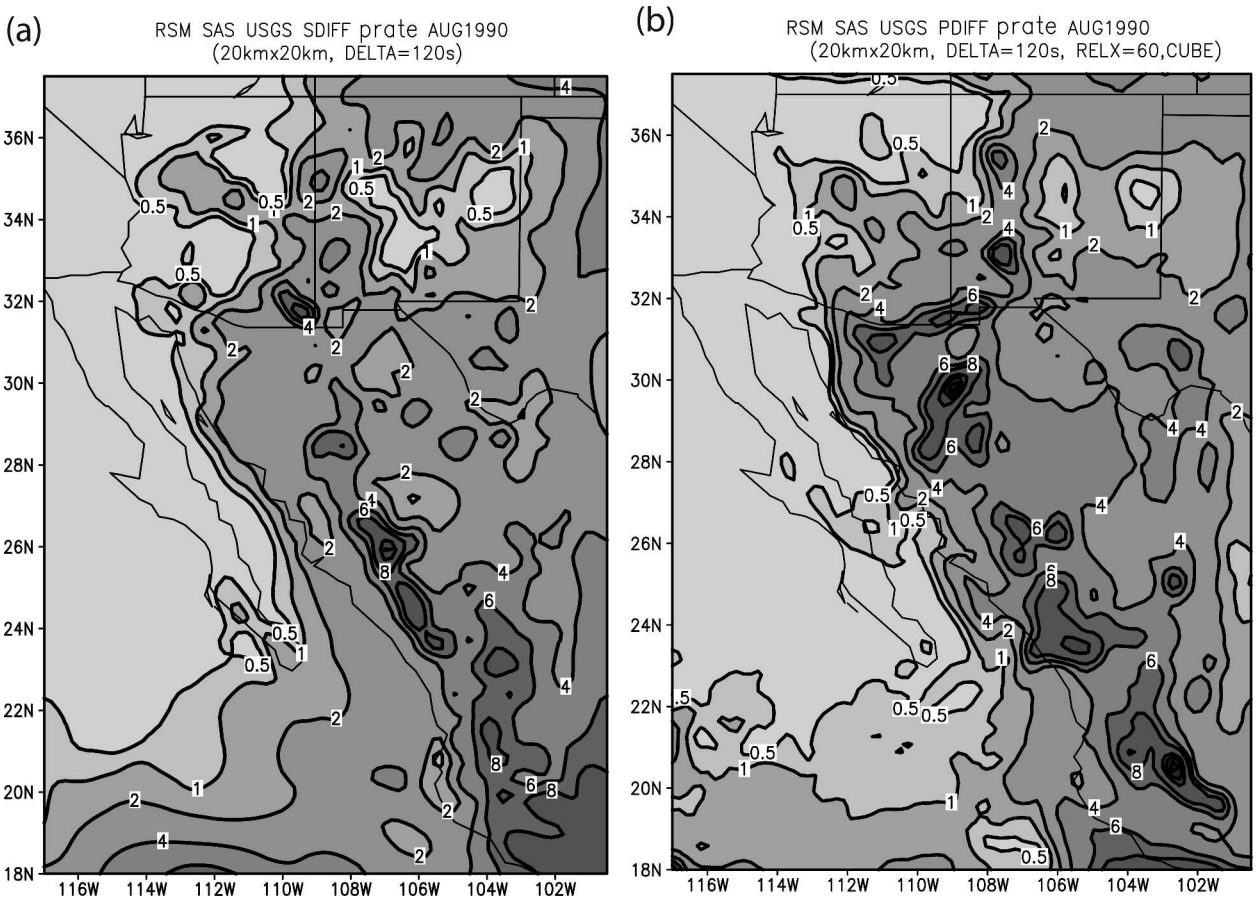

FIG. 15. Monthly averaged model rainfall in mm day^{-1} with contours of 0.5, 1, 2, 4, 6, 8, 10 mm day^{-1} from (a) the experiment with perturbation fourth-order horizontal diffusion on sigma surfaces and (b) the experiment with full-field second-order horizontal diffusion on pressure surfaces.

We solved this spurious diffusion problem by computing the process on pressure surfaces. To do this, we applied a coordinate transformation to variables on sigma coordinates and discretized the transformed diffusion terms. However, a caveat should be noted for this method. In addition to the original linear term, there are three nonlinear terms for second-order diffusion, or seven more for fourth-order diffusion. These nonlinear terms need to be computed in gridpoint space through a spectral transformation method. For the sake of simplicity and computational efficiency, the less scale-selective second-order scheme became a compromise. Nevertheless, the results from the second-order horizontal diffusion on pressure surfaces showed promising performance.

The advantage of using isobaric surfaces as the "horizontal" surfaces is that pressure is part of the model sigma coordinate. Therefore it is easier and simpler to perform a coordinate transform to pressure surfaces than to physical height surfaces. Although an isobaric surface is not generally truly horizontal but rather a quasi-horizontal surface, the results of this paper indicate that it is sufficient to produce well-behaved forecasts and simulations. Alternatively, Zängl (2002) suggested using horizontal diffusion on height surfaces, by interpolation of values on sigma surface to height surfaces, instead of via a discretized coordinate transformation. The one-side computation along the steep mountain slope without explicit extrapolation in his method is analogous to our coordinate transform, which does not explicitly extrapolate values beneath the ground either. Zängl's method is reasonable for implementation in finite-difference models. However, it may not be suitable for spectral models, such as RSM/MSM.

The cases were collected from various RSM/MSM user groups. Each case has its unique characteristics and provides a diversified test of the diffusion schemes. The opposite large-scale forcing of the Taiwan moist unstable case and the Hawaii stable case provide contrasting responses of the erroneous flow pattern through the horizontal diffusion on sigma surfaces. The wintertime Taiwan case with a prevailing northeasterly acted as a mesoscale or local-scale winter monsoon in

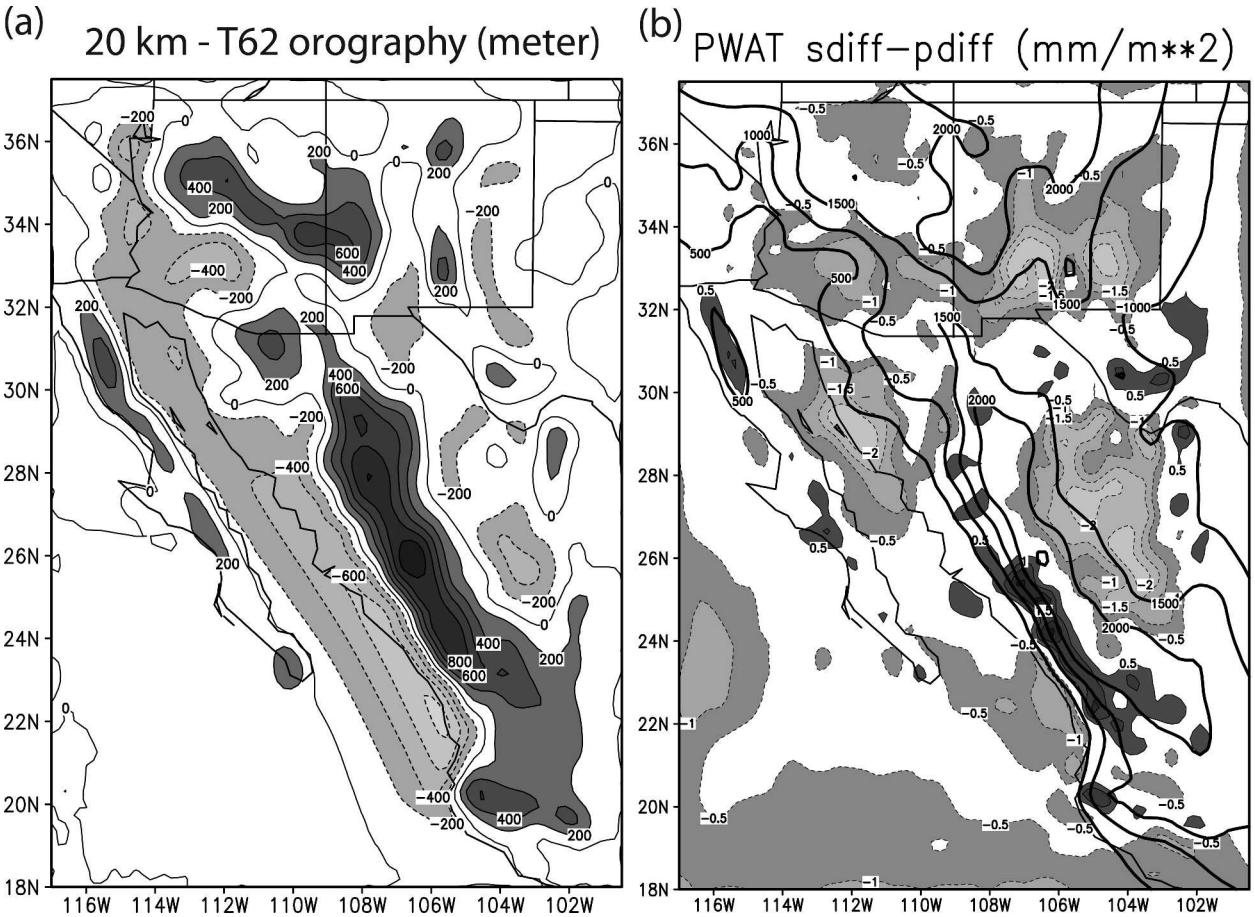

FIG. 16. (a) The terrain difference between 20-km RSM and T62 GSM with a contour interval of 200 m. (b) Monthly averaged difference of total precipitable water, in mm with a contour interval of 0.5 mm, between the experiment with perturbation fourth-order horizontal diffusion on sigma surfaces and the experiment with full-field second-order horizontal diffusion on pressure surfaces; heavy solid curves are the model terrain as in Fig. 7b.

contrast to the North American summer monsoon case. Both the Taiwan and Hawaiian cases have simple, island type of topography, but the North American case provides a continental condition with complex mountains. In all cases, simulation or forecast results with the horizontal diffusion on pressure surfaces showed improvement over the horizontal diffusion on sigma surfaces.

Under a conditional unstable ambient condition, the atmosphere was likely to be saturated and therefore induce further upward motion and low-layer convergence. As a result, the erroneous portion of warming and moistening air on mountain tops by the horizontal diffusion on sigma surfaces was reinforced by the condensation-induced additional low-level convergence, and hence produced excessive rainfall, as demonstrated in the Taiwan case and the North American case over the Sierra Madre Occidental. In a normal stratification under stable condition, however, the ambient atmosphere prevented the artificially diffused air from being ventilated. Therefore the erroneous portion of cooling and drying air accumulated and was enhanced, resulting in cold air flowing downhill to the flat ocean surface, as seen in the Oahu case and the North American case over Baja California.

The spurious flow produced by perturbation diffusion in the s-DIFF simulation is due to the large differences in orography between the RSM/MSM and their outer models. One obvious way to retain the original well-defined perturbation diffusion and yet generate less error is to downscale gradually. However, this would require immense computing power for handling multinested grids, especially for regional climate simulations or forecasts. We suggest a solution by computing diffusion on pressure surfaces based on a discretized coordinate transformation. Results shown here provide examples of how this approach can improve such mesoscale models. However, our method probably works best only for NCEP RSM/MSM or RSM-like spectral models. It should be noted that the less scale-selective second-order diffusion must be chosen for the sake of avoiding more time-consuming nonlinear computation.

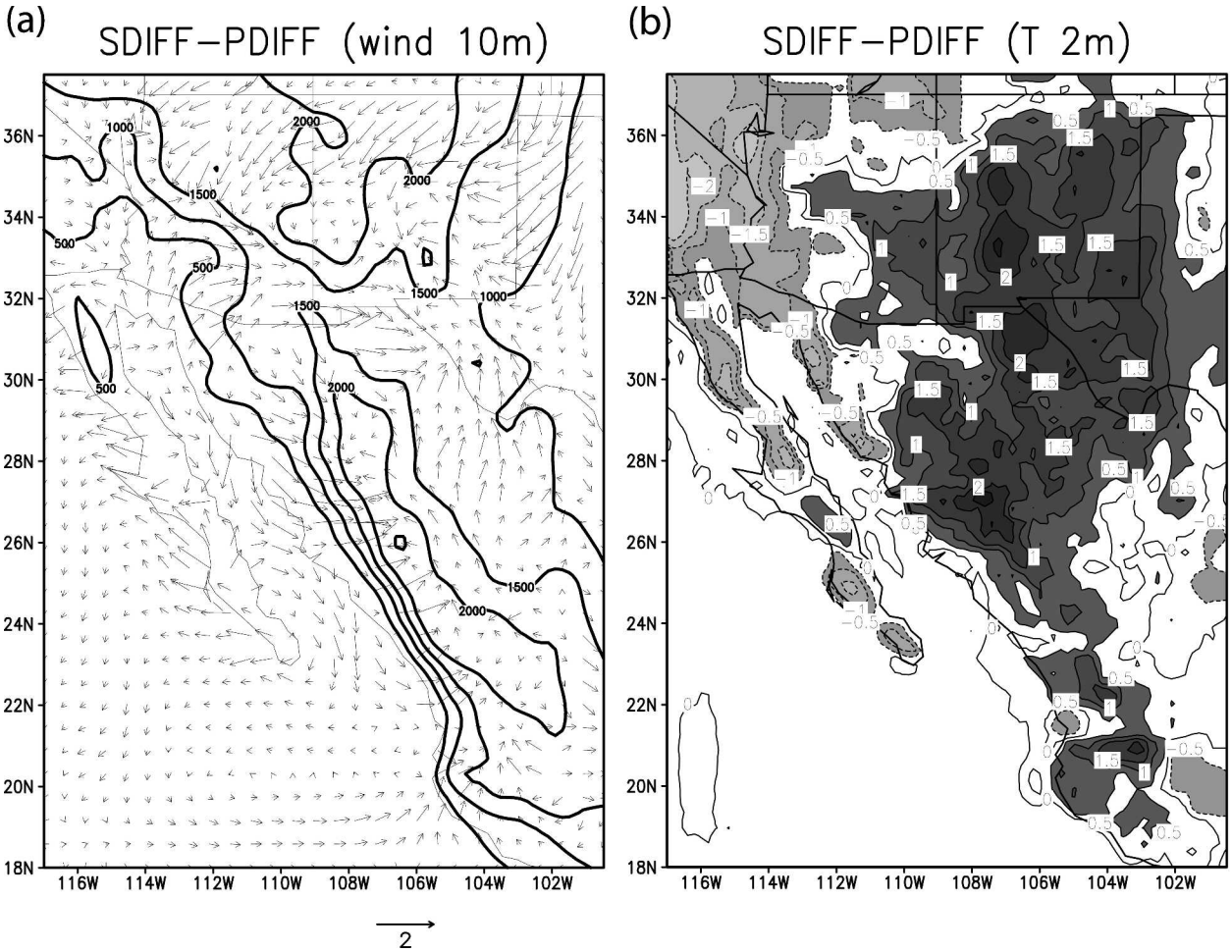

FIG. 17. The monthly differences between the experiment with perturbation fourth-order horizontal diffusion on sigma surfaces and the experiment with full-field second-order horizontal diffusion on pressure surface for (a) 10-m wind in m s^{-1}, where solid curves are model terrain as in Fig. 10b, and (b) 2-m temperature with a contour interval of 0.5 K.

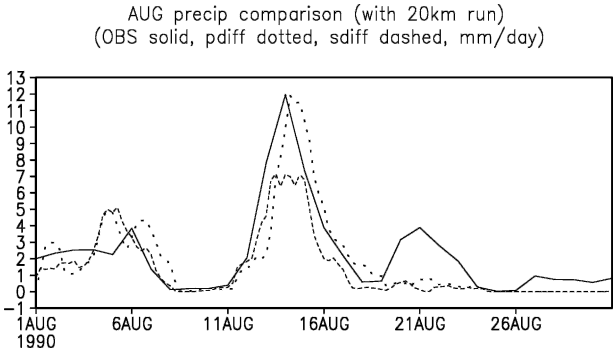

FIG. 18. The daily averaged rainfall rates in mm day^{-1} during Aug 1990 over the states of Arizona and New Mexico from observation (solid curve), the experiment with full-field second-order horizontal diffusion on pressure surfaces (dotted curve), and the experiment with perturbation fourth-order horizontal diffusion on sigma surfaces (dashed curve).

Also, the additional nonlinear terms prevent the use of a stable implicit scheme in updating the rate of change due to diffusion, and the less stable explicit time scheme might have shortcomings. Future improvement should be considered.

Acknowledgments. The implementation of this horizontal diffusion scheme on pressure surfaces was inspired by numerous discussions about the erroneous results over mountain areas with various researchers participating in previous RSM International Workshops, which have been supported by NOAA, USFS, NASA, and NSF. The Taiwan cases were performed on a Compaq XP1000 provided by the Department of Atmospheric Science, National Taiwan University (NTU), and the work is supported under Grants NSC 91-2111-M-002-021 and NSC 91-2621-Z-002-004. The Oahu simulations were carried out on a Dec Alpha Server ES40 that was purchased by the National Weather Service Pacific Region (NWSPR) for the Department of

Meteorology, University of Hawaii, in support of the collaboration between the university and the NWSPR, and the work is supported by NOAA through the UCAR COMET Outreach Program under Grants UCAR S99-98916 and UCAR S98-93859. North American experiments were conducted on IBM SP at NCEP, and the work is supported under Grant OGP/GAPP GC02-102. The authors thank NCEP internal reviewers, Drs. Sajal Kar and Shrinivas Moorthi, for their suggestions in improving the readability of the manuscript. We also extend our gratitude to Ms. Diane Boomer for proofreading the manuscript. The authors thank Dr. Dave Dempsey and another anonymous reviewer for their constructive comments and suggestions, and especially for their detailed and helpful annotations in the manuscript.

REFERENCES

Anderson, B. T., J. Roads, S.-C. Chen, and H.-M. H. Juang, 2000: Regional simulation of the low-level monsoon winds over the Gulf of California and southwestern United States. *J. Geophys. Res.,* **105,** 17 955–17 969.

Arakawa, A., 1966: Computational design for long-term numerical integrations of the equations of atmospheric motion. *J. Comput. Phys.,* **1,** 119–143.

Chen, Y.-L., Y. Zhang, S.-Y. Hong, K. Kodama, and H.-M. H. Juang, 2003: Validations of the NCEP MSM coupled with the NOAH LSM over the Hawaiian Islands. Preprints, *Fifth Symp. on Fire and Forest Meteorology,* Orlando, FL, Amer. Meteor. Soc., CD-ROM, 4.1.

Cullen, M. J. P., 1976: On the use of artificial smoothing in Galerkin and finite difference solution of the primitive equations. *Quart. J. Roy. Meteor. Soc.,* **102,** 77–91.

Juang, H.-M. H., 1988: Numerical simulations of the rapid cyclongenesis over Canada and evolution of a cold front observed on 25–26 April 1979 (SESAME-AVE-III). Ph.D. dissertation, University of Illinois at Urbana–Champaign, 223 pp. [Available from Department of Atmospheric Sciences, University of Illinois at Urbana–Champaign, 105 Gregory Avenue, Urbana, IL 61801.]

——, 2000: The NCEP mesoscale spectral model: The revised version of the nonhydrostatic regional spectral model. *Mon. Wea. Rev.,* **128,** 2329–2362.

——, and M. Kanamitsu, 1994: The NMC nested regional spectral model. *Mon. Wea. Rev.,* **122,** 3–26.

——, and S.-Y. Hong, 2001: Sensitivity of the NCEP regional spectral model on domain size and nesting strategy. *Mon. Wea. Rev.,* **129,** 2904–2922.

——, ——, and M. Kanamitsu, 1997: The NCEP regional spectral model: An update. *Bull. Amer. Meteor. Soc.,* **78,** 2125–2143.

Kalnay, E., and Coauthors, 1996: The NCEP/NCAR 40-Yr Reanalysis Project. *Bull. Amer. Meteor. Soc.,* **77,** 437–471.

Kanamitsu, M., and Coauthors, 1991: Recent changes implemented into the global forecast system at NMC. *Wea. Forecasting,* **6,** 425–435.

——, and Coauthors, 2002: NCEP-DOE AMIP-II reanalysis (R-2). *Bull. Amer. Meteor. Soc.,* **83,** 1631–1643.

Moorthi, S., 1997: NWP experiments with a grid-point semi-Lagrangian semi-implicit global model at NCEP. *Mon. Wea. Rev.,* **125,** 74–98.

Phillips, N. A., 1959: An example of non-linear computational instability. *The Atmosphere and Sea in Motion: Rossby Memorial Volume*, E. Bolin, Ed., Rockefeller Institute Press, 501–504.

Pielke, R. A., 1984: *Mesoscale Meteorological Modeling.* Academic Press, 612 pp.

Robert, A., 1993: Bubble convection experiments with a semi-implicit formulation of the Euler equations. *J. Atmos. Sci.,* **50,** 1865–1873.

Sardeshmukh, P. D., and B. J. Hoskins, 1984: Spatial smoothing on the sphere. *Mon. Wea. Rev.,* **112,** 2524–2529.

Shapiro, R., 1970: Smoothing, filtering and boundary effects. *Rev. Geophys. Space Phys.,* **8,** 359–387.

Tag, P. M., F. W. Murray, and L. R. Kening, 1979: A comparison of several forms of eddy viscosity parameterization in a two-dimensional cloud model. *J. Appl. Meteor,* **18,** 1429–1441.

von Storch, H., 1978: Construction of optimal numerical filters fitted for noise damping in numerical simulation models. *Contrib. Atmos. Phys.,* **51** (2), 189–197.

Zängl, G., 2002: An improved method for computing horizontal diffusion in a sigma-coordinate model and its application to simulations over mountainous topography. *Mon. Wea. Rev.,* **130,** 1423–1432.